Letter

# Dominant Processes of HONO Derived from Multiple Field Observations in Contrasting Environments

Ying Jiang, Likun Xue,* Hengqing Shen,* Can Dong, Zhisheng Xiao, and Wenxing Wang

Cite This: *Environ. Sci. Technol. Lett.* 2022, 9, 258–264

Read Online

ACCESS | Metrics & More | Article Recommendations | SI Supporting Information

**ABSTRACT:** The sources of atmospheric nitrous acid (HONO) have been frequently investigated in recent decades. However, the dominant mechanisms of HONO formation and its significant daytime source in contrasting environments remain largely unknown. In this study, 46 observational data sets were collected worldwide, and the underlying processes driving diurnal HONO patterns were extracted on the basis of principal component analysis (PCA). We identified three dominant processes: a $NO_x$ process (PC1) that was dominant in polluted inland areas, a photodecomposition process (PC2) that was dominant in marine or mountain environments, and a soil-related process (PC3). The three processes together explained >88% of the total variance. HONO variations in coastal regions were governed by either PC1 or PC2, determined by the effects of the sea−land breeze. These PCs were then applied to the identification of unknown HONO sources. The results showed that the unknown source was mainly related to the $NO_x$ process in most urban areas; however, it was associated with the photodecomposition-dominated process in coastal regions. The application of PCA to isolate the common behaviors of HONO provides valuable insights into the dominant HONO formation processes in different environments.

**KEYWORDS:** *nitrous acid, principal component analysis, $NO_x$ process, photodecomposition process, soil-related process*
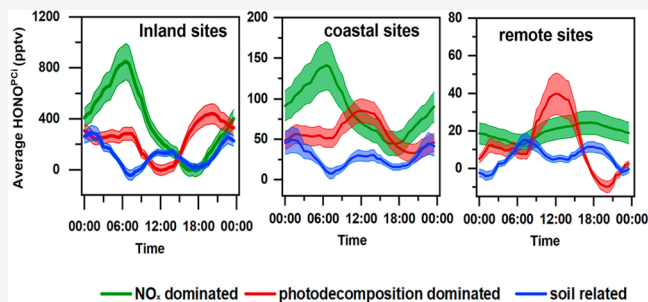
## INTRODUCTION

Nitrous acid (HONO), a major hydroxyl radical (OH) reservoir, plays a vital role in atmospheric photochemistry. The photolysis of HONO can contribute over 90% of primary OH production during the daytime.[1−4] HONO can be either directly emitted from combustion[5] and soil microbial processes[6,7] or formed by gas-phase and heterogeneous reactions on wet or reduced surfaces involving nitrogen oxides ($NO_x$ = NO + $NO_2$) or by photolysis of nitrogen-containing compounds and particulate nitrate ($pNO_3^-$).[8−11] Photolysis and reaction with OH are the main HONO sinks in the daytime, whereas deposition dominates at night in the boundary layer.[12,13] Although significant advances have been made in the study of HONO sources over the past few decades, the ambient concentrations of HONO, especially in the daytime, are usually largely underestimated by models, and the dominant HONO processes in contrasting environments remain controversial.

Diurnal HONO behavior is a composite of its sources and sinks, thereby reflecting the characteristics of the observed environments, including pollution levels, meteorological conditions, and physical and chemical processes. Diurnal HONO concentrations generally show a "groove" shape with lower concentrations in the daytime, the lowest concentration at noon, and higher concentrations at night in most urban and semiurban areas.[14−16] Nevertheless, the opposite pattern, with concentration peaks at noon and lower levels at night, has been observed in many mountain and remote marine regions.[8,17] Other diurnal variations different from these two typical patterns have also been reported.[18−20] Identifying the dominant processes that control these diurnal behaviors is important for gaining insights into the underlying sources and sinks of HONO.

Principal component analysis (PCA) is an effective data reduction technique. It identifies the primary behaviors (patterns) by transforming original data into a few linear combinations while retaining the variation (information) present in the data set as much as possible.[21−23] This method has been widely applied to explore the dominant air pollution sources; for example, it was successfully used to isolate the regional background ozone in Houston and elucidate the major sources of volatile organic compounds and fine particles in various environments.[24−26] However, it has never been applied to ambient HONO studies, which have proposed many different sources and sinks of HONO. In this study, we
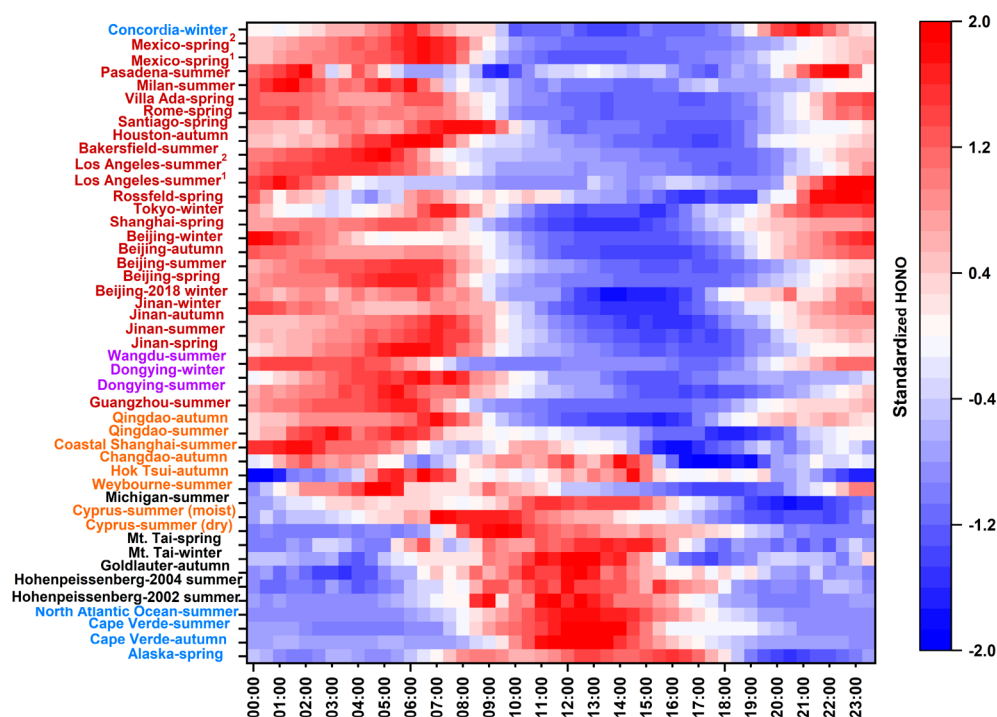
**Figure 1.** Temporal distribution of standardized HONO mixing ratios of the 46 global observation data sets. Standardized HONO $= \frac{HONO - \overline{HONO}}{\delta_{HONO}}$, where $\overline{HONO}$ and $\delta_{HONO}$ are the mean and standard deviation, respectively, of diurnal HONO data at each site. Red, purple, orange, black, and blue colors represent urban/suburban, rural, coastal/island, mountain/forest, and marine/remote, respectively. The detailed information about these observation sites is provided in the Supporting Information.

attempted to use PCA for the first time to explore the dominant HONO processes in contrasting environments based on 46 global diurnal HONO data sets. The derived principal components (PCs) were applied to analyze the unknown daytime HONO source(s). The findings of this study provide valuable insights to distinguish discrepancies between major HONO sources in different ambient atmospheres and illustrate that statistical methods can be widely applied to data mining in atmospheric chemistry studies.

### ■ MATERIALS AND METHODS

**Observational Data.** Diurnal HONO data from 46 observational data sets at 31 sites, including 17 inland (urban or rural) sites, six coastal or island sites, four mountain/forest sites, and four marine/remote sites, were collected from published literature and our measurements (Figure S1 and Table S1). More details about these data sets can be found in the original literature.[8,9,14,15,17−20,27−46] In general, 21 of the observational data sets were extracted from observations conducted inside China and most of the rest from observations conducted inside North America or Europe. Our group conducted 13 observations with more available parameters, which are used to explore daytime HONO sources further. The additional parameters used for the unknown source analysis are listed in Table S2. Diurnal HONO data from these observations were extracted for PCA with a time resolution of 30 min.

**Principal Component Analysis.** The obtained diurnal HONO data were standardized using eq 1 to avoid biasing the influence of certain variables:

$$HONO_{std} = \frac{HONO - \overline{HONO}}{\delta_{HONO}} \tag{1}$$

where $\overline{HONO}$ and $\delta_{HONO}$ are the average and standard deviation, respectively, of the diurnal HONO data for each observation.

PCA was performed using SPSS 20 software (SPSS Inc., Chicago, IL) on the correlation matrix and varimax rotation. The diurnal HONO data were suitable for PCA according to the Kaiser−Meyer−Olkin (KMO) and Bartlett's test (KMO > 0.6, and $p < 0.001$) (Table S3). Three principal components were derived, explaining >88% of the total variance in these data sets. The first principal component (PC1) explained 45% of the variance, and the second and third components explained an additional 29% and 14%, respectively (Table S4). Details concerning PCA and the calculation process are provided in the Supporting Information.

### ■ RESULTS AND DISCUSSION

**Diurnal Variations in HONO.** The HONO mixing ratios of these observations vary by several orders of magnitude, with the highest levels observed at urban sites (e.g., average of 2.24 ppbv in autumn Beijing), followed by those at rural or coastal sites, and the lowest values were observed in mountain or marine atmospheres (e.g., approximately 1.3 pptv at autumn Cape Verde of the marine environment). The observed HONO concentrations in China are generally higher than those observed in other areas of the same type. For example, the HONO concentration at Mt. Tai in China is higher (146.9 pptv in winter[17]) than those at other high-elevation sites (approximately 61.1 pptv in Hohenpeissenberg, Germany, and 61.6 pptv in Goldlauter, Germany[29]).

Figure 1 shows the diurnal variations in standardized HONO concentrations of these 46 observational data sets. The HONO concentrations present a typical "groove" shape at most ground-level urban/rural sites, with higher concentrations in the nighttime and lower concentrations in the daytime, indicating significant accumulation and rapid consumption during the night and day, respectively. In contrast, the HONO concentrations at marine and mountain sites display an opposite trend with a peak concentration at noon, thereby revealing a more significant daytime source. The diurnal HONO patterns over some coastal sites show two peaks, indicating the potential effects of sea−land breezes on HONO behaviors and/or additional daytime HONO sources. While the difference in the average $HONO/NO_2$ ratio (0.02−0.11) is relatively small in most environments (Figure S2), the diurnal $HONO/NO_2$ patterns in these observations are even more complex, with peaks occurring at night, in the morning, or at noon.[15,17] These completely different diurnal variations illustrate different dominant HONO processes in different environments.

**Dominant HONO Processes Extracted by PCA.** Figure 2 shows the spatial distribution of the component loadings [coefficients (Figure 2a)] and time series of the PC scores [amplitudes (Figure 2b)] for the derived PC1−PC3. The loadings represent the mean contribution of each component to HONO diurnal variation in each observation, and the scores represent the time dependence of the relative contribution, which was acquired by projecting the measured data onto the new rotation axes defined by the PCs. The underlying chemical and physical processes could be inferred by comparing the spatial and temporal information provided by the loadings and scores with meteorological parameters, precursors, and specific indicators (Figure S3 and Table S5). As an orthogonal transformation method, it should be noted that the dominant processes of HONO represented by PCs should be uncorrelated or independent of each other.

PC1 is identified as a $NO_x$-dominated process according to its positive and strong loadings at most polluted ground-level sites (Figure 2a) and strong correlations [$r > 0.58$ (Figure S3a and Table S5)] with $NO_x$. This speculation is also supported by the work of Fu et al.,[47] who reported that $NO_x$-related processes were the largest contributor to HONO formation over the polluted areas of southern China, especially at night. An interesting finding in Figure S3a is that, while PC1 shows strong correlations with $NO_2$ in most polluted sites, their correlation in heavily polluted urban sites (Beijing in 2018 winter, Jinan in winter, and Jinan in autumn) with high NO concentrations (daily average mixing ratio of NO of over 33 ppbv in Jinan in winter) is weak. Meanwhile, the correlations of PC1 with NO in these three sites are strong ($r > 0.7$). Because the contribution of direct vehicle emission is relatively small,[48,49] this result may reflect, to a greater extent, the recent finding that the gas-phase reaction of NO and OH plays a more vital role in heavily polluted regions.[4,13,50,51] PC1 exhibited a strong and positive relationship with relative humidity (RH), suggesting a potential promotional role of water vapor in HONO formation.[52] When considering the radiation impacts, we compared the higher and even positive coefficients between PC1 and $J_{NO_2} \times NO_2$ ($\times PM_{2.5}$) (as indicators of photoenhanced heterogeneous reactions of $NO_2$) with the negative coefficients between PC1 and $PM_{2.5} \times J_{NO_2}$ (as an indicator of nitrate photolysis), indicating that PC1 is
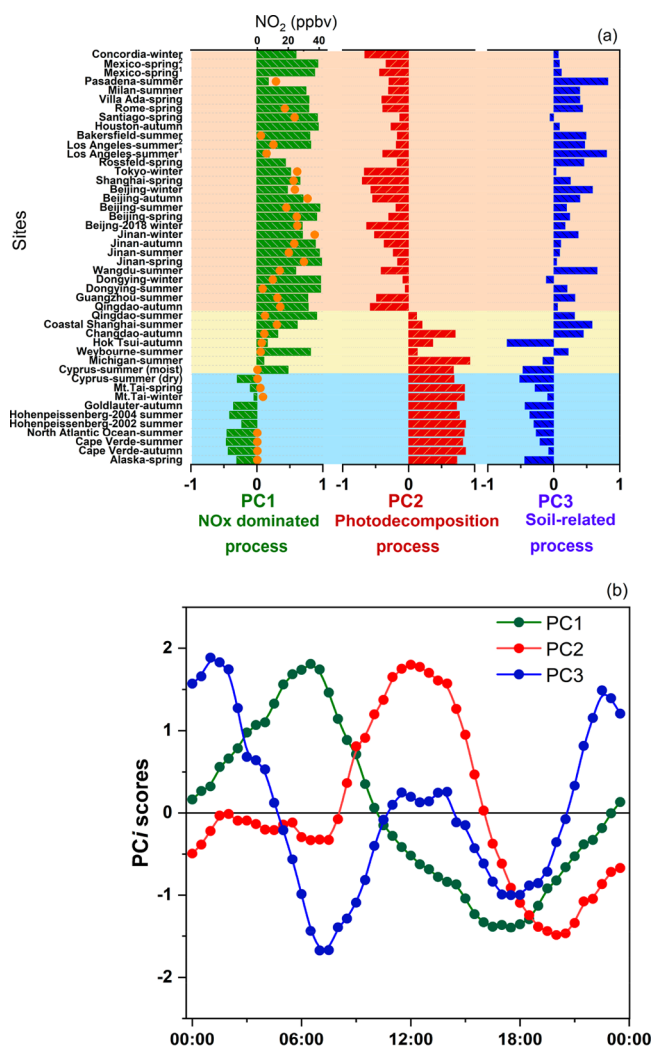


**Figure 2.** Spatial distribution of the (a) loadings and (b) time series of the scores for the three derived principal components. The background colors in panel (a) divided these observations into three clusters according to the loadings and site type. Cluster 1 (pink shade) possesses positive loadings and negative loadings for PC1 and PC2, respectively, including most inland sites with one peak at night. Cluster 2 (light yellow shade) possesses positive loadings for both PC1 and PC2, including mainly coastal and island sites. Cluster 3 (light blue shade) possesses negative loadings and positive loadings for PC1 and PC2, respectively, including mainly marine and mountain sites with one peak at noon.

not a composite of nonphotolytic mechanisms but a process coupling in which $NO_x$ participates and acts as a decisive factor. Overall, PC1 is considered a $NO_x$-dominated process (including HONO formation through the reactions associated with NO and $NO_2$, photoenhanced heterogeneous reactions of $NO_2$, and even direct emission).

PC2 is identified as a photodecomposition-dominated process according to its noontime peak (Figure 2b) and its high correlation with radiation-related parameters [$r > 0.86$ for its correlations with $J_{NO_2}$ (Figure S3b and Table S5)]. On the basis of its weak correlations with $NO_x$ and the features of PCA showing that PC2 is unrelated to PC1 (a process dominated by $NO_x$), it could be confirmed that $NO_x$ is not an important factor in PC2. Except for $NO_x$, $pNO_3^-$[8,9] and nitrogen-containing compounds[11] are also considered to play
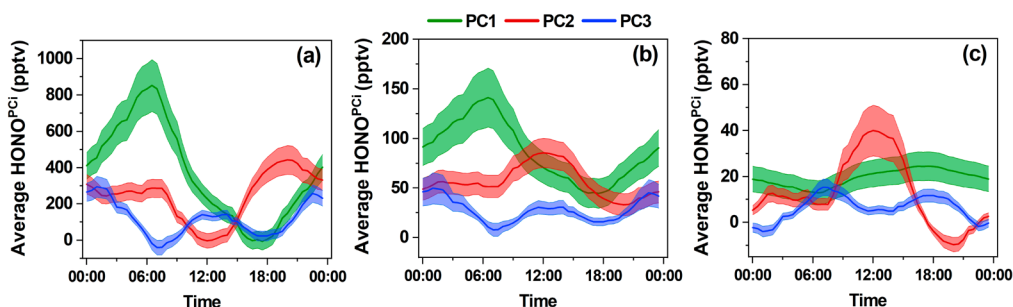
**Figure 3.** Average nitrous acid (HONO) concentrations contributed by PC1−PC3 for (a) cluster 1, (b) cluster 2, and (c) cluster 3. The lines represent the average HONO concentrations contributed by PC1−PC3. The shaded areas represent one-quarter of the standard deviation.

important roles in HONO formation. Field observations and model simulations have suggested that $pNO_3^-$ photolysis sustains the observed HONO concentrations at noon in typical marine and mountain environments.[8,53] The higher correlation coefficients of PC2 with $PM_{2.5} \times J_{NO_2}$ compared with $NO_2 \times PM_{2.5} \times J_{NO_2}$ (e.g., $r = 0.84$ and $0.63$, respectively, in Qingdao in summer) further indicate that PC2 is a process unrelated to $NO_x$. In all reported sites, PC2 showed a higher correlation with $PM_{2.5} \times J_{NO_2}$ (a measure of nitrate photolysis) than with $NO_2 \times J_{NO_2}$ (a measure of $NO_2$ photoenhanced reactions) (e.g., $r = 0.83$ and $0.78$, respectively, in Jinan in summer). We infer PC2 as a process dominated by photodecomposition of $pNO_3^-$ and nitrogen-containing compounds. This process plays a vital role in relatively clean sites, such as marine or mountain areas (Figure 2a). Noting that the photolysis of $pNO_3^-$ may also play a role in HONO formation in urban or rural areas, a recent study by Cui et al.[54] demonstrated the significance of $NO_3^-$ concentration compared with $NO_2$ column density for HONO prediction in China. However, the rapid HONO photolysis may mask the importance of the photochemical process, which is reflected in the general negative loading of PC2 in polluted areas (Figure 2a).

PC3 exhibits an even more complex spatial and temporal pattern. Positive loadings of PC3 are found at most urban or coastal sites, whereas negative loadings at most marine or mountain sites. Thus, we tend to consider PC3 as a soil-related process, including the soil emission process and the HONO uptake or dry deposition process. The relatively strong positive correlations between PC3 and RH further support our hypothesis, as the previous study has pointed out that soil emissions of HONO were enhanced under high-RH conditions.[37] Large positive loadings found in agriculturally influenced sites (e.g., Wangdu in summer and Pasadena in summer) are also consistent with the property of this source. The two peaks of the diurnal variations of PC3 at day and night may be controlled by the RH and sunlight,[55] respectively. Indeed, this process has been recognized as a vital HONO source since the study of Su et al.[6,7] Overall, PC3 is ascribed to a soil-related process.

According to the loadings of PC1, PC2, and the site type, we divided the 46 observation data sets into three clusters. Cluster 1 possesses positive and negative loadings for PC1 and PC2, respectively, including most of the relatively polluted inland sites (Mexico City, Los Angeles, Rome, Santiago, Houston, Bakersfield, Rossfeld, Tokyo, Concordia, Shanghai, Beijing, Jinan, Wangdu, Dongying, Guangzhou, and Qingdao in autumn affected by continental air masses) with one peak at night. Cluster 2 possesses positive loadings for both PC1 and

PC2, including mainly coastal and island sites [coastal Shanghai, Changdao, Hok Tsui, Weybourne, Michigan, Cyprus (moist) affected by sea breeze, and Qingdao in summer affected by marine air masses]. Cluster 3 possesses negative loadings and positive loadings for PC1 and PC2, respectively, including mainly marine and mountain sites [Cyprus (dry) with potentially more physical $NO_y$ accumulation,[37] Mt. Tai, Cape Verde, Alaska, North Atlantic Ocean, Hohenpeissenberg, and Goldlauter] with one peak at noon. It should be noted that the remote site of Concordia also shows a strong and positive loading of PC1, which is the opposite of other remote sites. This could be explained by the potential overestimation of HONO due to the presence of $HNO_4$ at Concordia,[56] leading to a higher HONO concentration at night (Figure 1).

To clarify the relative importance of the dominant processes that control the diurnal behaviors of HONO, we calculated the average contribution of PC$i$ ($i$ = 1, 2, or 3) over different cluster sites (in contrasting environments). The detailed calculation process is documented in the Supporting Information. Even the same PC shows different behaviors in contrasting environments. For example, the diurnal HONO pattern contributed by PC2 displays a "groove" shape with a lower value in the daytime at inland sites (cluster 1), whereas it shows a daytime peak at coastal and marine areas (clusters 2 and 3). This discrepancy could be attributed to the relative contributions of photorelated reactions, namely, potentially stronger photorelated sinks at cluster 1 sites and stronger photorelated sources at cluster 2 and cluster 3 sites. The daytime peak of PC2 reveals common sources of HONO in marine or coastal areas. Overall, the ambient HONO concentrations are determined mainly by the $NO_x$-dominated, photodecomposition-dominated, and soil-related processes. The $NO_x$ process is prominent in the inland urban and rural areas, whereas the photodecomposition process is dominant in the marine and mountain areas. For coastal regions, due to sea−land circulation, the $NO_x$ process is dominant at night, whereas the photodecomposition process contributes significantly in the daytime. The contribution of PC3 is relatively minor at these three clusters. The $NO_x$-dominated process has been intensively studied. Although the photodecomposition process has been proposed to account for the daytime HONO peak observed in the coastal or marine atmosphere,[8,20] its detailed mechanism requires further investigations. Obviously, the PCA method provides a visual indication of the patterns of variation of HONO in different atmospheres and offers insights into the universally dominant processes driving ambient HONO variations.

**Implications for an Unknown HONO Source.** Previous studies have suggested that a strong HONO source exists in

the daytime, which could not be explained by direct emissions or the gas-phase reaction of NO + OH. Thus, a budget analysis was conducted to explore the potential unknown HONO source(s) and examine its relationship with the PCs derived above. Detailed information about the step-by-step method to calculate the HONO budget and the relevant parameters (e.g., OH concentration and photolysis rate) is provided in Text S1, and the diurnal HONO production and loss rates are presented in Figure S4.

A strong potential unknown HONO production rate ($P_{other}$) ranging from 0.3 to 4.5 ppbv/h exists at all sites. We explored the relationship of $P_{other}$ with the three isolated PCs. The results of the correlation analysis between $P_{other}$ and the scores of PC1−PC3 are provided in Table S7. The $P_{other}$ of the sites in cluster 1 (inland sites except for Jinan in winter) shows a more significant positive correlation with PC1 than with PC2 and PC3 (e.g., $r$ = 0.72, 0.30, and −0.15 for PC1−PC3, respectively, in Jinan in spring), thereby revealing the potential importance of the $NO_x$-dominated process. The correlations between $P_{other}$ and PC2 are extremely strong at coastal and mountain sites (e.g., $r$ = 0.95 with PC2 in Mt. Tai in spring), indicating that the photodecomposition-dominated process plays a vital role at these sites, which is consistent with the significant correlations between $P_{other}$ and $J_{NO_2}$. The correlation results between $P_{other}$ and the scores of PC$i$ in this study are consistent with the results of the traditional correlation analysis using specific indicators, thereby further revealing the role of PCA in distinguishing potential HONO sources and confirming our speculation about the meaning of each PC.

This study used PCA for the first time to systematically analyze the HONO observation data from multiple sites worldwide, providing an understanding of the dominant processes driving ambient HONO concentrations in different environments. The results illustrate that $NO_x$-dominated, photodecomposition-dominated, and soil-related processes have important effects on the sources and sinks of ambient HONO and provide intuitive proof that sea−land circulation plays an important role in HONO formation at coastal sites. It is noteworthy that the 46 observation data sets may not cover all environments and, to some extent, reduce the representativeness of the PCA results. More observations, especially from less polluted marine and high-elevation sites as well as different pollution cases in different areas, are urgently needed, and further laboratory investigation of HONO formation through the photodecomposition pathway is required. The PCA approach is successfully used to investigate the potential daytime HONO source(s) for the first time. Our results demonstrate that despite the different characteristics and variation patterns of ambient HONO observed in various environments, the underlying dominant processes affecting HONO formation and sinks are quite simple. We also provide guidance for the future investigations of potential unknown source(s) of HONO in different types of areas.

## ASSOCIATED CONTENT

### Supporting Information

The Supporting Information is available free of charge at https://pubs.acs.org/doi/10.1021/acs.estlett.2c00004.

> Method of calculation of the HONO budget and contribution from each PC$i$; spatial distribution of measurement sites and sampling information; related parameter, HONO budget results, and information used

for HONO budget analysis; results of KMO and Bartlett's test and PCA; and correlation coefficients between PC$i$ and parameters and $P_{other}$ (PDF)

## AUTHOR INFORMATION

### Corresponding Authors

**Likun Xue** − *Environment Research Institute, Shandong University, Qingdao, Shandong 266237, China;* orcid.org/0000-0001-7329-2110; Email: xuelikun@sdu.edu.cn

**Hengqing Shen** − *Environment Research Institute, Shandong University, Qingdao, Shandong 266237, China;* Email: hqshen@sdu.edu.cn

### Authors

**Ying Jiang** − *Environment Research Institute, Shandong University, Qingdao, Shandong 266237, China*

**Can Dong** − *Environment Research Institute, Shandong University, Qingdao, Shandong 266237, China*

**Zhisheng Xiao** − *School of Atmospheric Physics, Nanjing University of Information Science and Technology, Nanjing, Jiangsu 210044, China*

**Wenxing Wang** − *Environment Research Institute, Shandong University, Qingdao, Shandong 266237, China*

Complete contact information is available at:
https://pubs.acs.org/10.1021/acs.estlett.2c00004

### Author Contributions

L.X. designed the study and revised the manuscript. H.S. analyzed the data and revised the manuscript. Y.J. collected the data, performed the data analyses, and wrote the paper. C.D., Z.X., and W.W. helped in the interpretation of results.

### Notes

The authors declare no competing financial interest.

## REFERENCES

(1) Alicke, B.; Platt, U.; Stutz, J. Impact of nitrous acid photolysis on the total hydroxyl radical budget during the Limitation of Oxidant Production/Pianura Padana Produzione di Ozono study in Milan. *J. Geophys. Res.: Atmos.* **2002**, *107* (D22), LOP 9-1−LOP 9-17.

(2) Kleffmann, J.; Gavriloaiei, T.; Hofzumahaus, A.; Holland, F.; Koppmann, R.; Rupp, L.; Schlosser, E.; Siese, M.; Wahner, A. Daytime formation of nitrous acid: A major source of OH radicals in a forest. *Geophys. Res. Lett.* **2005**, *32* (5), L05818.

(3) Zhou, X.; Civerolo, K.; Dai, H.; Huang, G.; Schwab, J.; Demerjian, K. Summertime nitrous acid chemistry in the atmospheric boundary layer at a rural site in New York State. *J. Geophys. Res.: Atmos.* **2002**, *107* (D21), ACH 13-1−ACH 13-11.

(4) Gu, R.; Shen, H.; Xue, L.; Wang, T.; Gao, J.; Li, H.; Liang, Y.; Xia, M.; Yu, C.; Liu, Y.; Wang, W. Investigating the sources of

atmospheric nitrous acid (HONO) in the megacity of Beijing, China. *Sci. Total Environ.* **2022**, *812*, 152270.

(5) Theys, N.; Volkamer, R.; Muller, J. F.; Zarzana, K. J.; Kille, N.; Clarisse, L.; De Smedt, I.; Lerot, C.; Finkenzeller, H.; Hendrick, F.; Koenig, T. K.; Lee, C. F.; Knote, C.; Yu, H.; Van Roozendael, M. Global nitrous acid emissions and levels of regional oxidants enhanced by wildfires. *Nat. Geosci.* **2020**, *13* (10), 681−686.

(6) Su, H.; Cheng, Y.; Oswald, R.; Behrendt, T.; Trebs, I.; Meixner, F. X.; Andreae, M. O.; Cheng, P.; Zhang, Y.; Poschl, U. Soil nitrite as a source of atmospheric HONO and OH radicals. *Science* **2011**, *333* (6049), 1616−8.

(7) Oswald, R.; Behrendt, T.; Ermel, M.; Wu, D.; Su, H.; Cheng, Y.; Breuninger, C.; Moravek, A.; Mougin, E.; Delon, C.; Loubet, B.; Pommerening-Roser, A.; Sorgel, M.; Poschl, U.; Hoffmann, T.; Andreae, M. O.; Meixner, F. X.; Trebs, I. HONO emissions from soil bacteria as a major source of atmospheric reactive nitrogen. *Science* **2013**, *341* (6151), 1233−5.

(8) Ye, C.; Zhou, X.; Pu, D.; Stutz, J.; Festa, J.; Spolaor, M.; Tsai, C.; Cantrell, C.; Mauldin, R. L., 3rd; Campos, T.; Weinheimer, A.; Hornbrook, R. S.; Apel, E. C.; Guenther, A.; Kaser, L.; Yuan, B.; Karl, T.; Haggerty, J.; Hall, S.; Ullmann, K.; Smith, J. N.; Ortega, J.; Knote, C. Rapid cycling of reactive nitrogen in the marine boundary layer. *Nature* **2016**, *532* (7600), 489−491.

(9) Zhou, X.; Zhang, N.; TerAvest, M.; Tang, D.; Hou, J.; Bertman, S.; Alaghmand, M.; Shepson, P. B.; Carroll, M. A.; Griffith, S.; Dusanter, S.; Stevens, P. S. Nitric acid photolysis on forest canopy surface as a source for tropospheric nitrous acid. *Nat. Geosci.* **2011**, *4* (7), 440−443.

(10) Ziemba, L. D.; Dibb, J. E.; Griffin, R. J.; Anderson, C. H.; Whitlow, S. I.; Lefer, B. L.; Rappenglück, B.; Flynn, J. Heterogeneous conversion of nitric acid to nitrous acid on the surface of primary organic aerosol in an urban atmosphere. *Atmos. Environ.* **2010**, *44* (33), 4081−4089.

(11) Bejan, I.; Abd El Aal, Y.; Barnes, I.; Benter, T.; Bohn, B.; Wiesen, P.; Kleffmann, J. The photolysis of ortho-nitrophenols: a new gas phase source of HONO. *Phys. Chem. Chem. Phys.* **2006**, *8* (17), 2028−2035.

(12) Liu, Y. H.; Lu, K. D.; Li, X.; Dong, H. B.; Tan, Z. F.; Wang, H. C.; Zou, Q.; Wu, Y. S.; Zeng, L. M.; Hu, M.; Min, K. E.; Kecorius, S.; Wiedensohler, A.; Zhang, Y. H. A Comprehensive Model Test of the HONO Sources Constrained to Field Measurements at Rural North China Plain. *Environ. Sci. Technol.* **2019**, *53* (7), 3517−3525.

(13) Wong, K. W.; Oh, H. J.; Lefer, B. L.; Rappenglück, B.; Stutz, J. Vertical profiles of nitrous acid in the nocturnal urban atmosphere of Houston, TX. *Atmos. Chem. Phys.* **2011**, *11* (8), 3595−3609.

(14) Gu, R.; Zheng, P.; Chen, T.; Dong, C.; Wang, Y. n.; Liu, Y.; Liu, Y.; Luo, Y.; Han, G.; Wang, X.; Zhou, X.; Wang, T.; Wang, W.; Xue, L. Atmospheric nitrous acid (HONO) at a rural coastal site in North China: Seasonal variations and effects of biomass burning. *Atmos. Environ.* **2020**, *229*, 117429.

(15) Li, D.; Xue, L.; Wen, L.; Wang, X.; Chen, T.; Mellouki, A.; Chen, J.; Wang, W. Characteristics and sources of nitrous acid in an urban atmosphere of northern China: Results from 1-yr continuous observations. *Atmos. Environ.* **2018**, *182*, 296−306.

(16) Liu, Y. H.; Lu, K. D.; Dong, H. B.; Li, X.; Cheng, P.; Zou, Q.; Wu, Y. S.; Liu, X. G.; Zhang, Y. H. In situ monitoring of atmospheric nitrous acid based on multi-pumping flow system and liquid waveguide capillary cell. *J. Environ. Sci.* **2016**, *43*, 273−284.

(17) Jiang, Y.; Xue, L.; Gu, R.; Jia, M.; Zhang, Y.; Wen, L.; Zheng, P.; Chen, T.; Li, H.; Shan, Y.; Zhao, Y.; Guo, Z.; Bi, Y.; Liu, H.; Ding, A.; Zhang, Q.; Wang, W. Sources of nitrous acid (HONO) in the upper boundary layer and lower free troposphere of the North China Plain: insights from the Mount Tai Observatory. *Atmos. Chem. Phys.* **2020**, *20* (20), 12115−12131.

(18) Elshorbany, Y. F.; Kurtenbach, R.; Wiesen, P.; Lissi, E.; Rubio, M.; Villena, G.; Gramsch, E.; Rickard, A. R.; Pilling, M. J.; Kleffmann, J. Oxidation capacity of the city air of Santiago, Chile. *Atmos. Chem. Phys.* **2009**, *9* (6), 2257−2273.

(19) Wen, L.; Chen, T.; Zheng, P.; Wu, L.; Wang, X.; Mellouki, A.; Xue, L.; Wang, W. Nitrous acid in marine boundary layer over eastern Bohai Sea, China: Characteristics, sources, and implications. *Sci. Total Environ.* **2019**, *670*, 282−291.

(20) Yang, J.; Shen, H.; Guo, M.-Z.; Zhao, M.; Jiang, Y.; Chen, T.; Liu, Y.; Li, H.; Zhu, Y.; Meng, H.; Wang, W.; Xue, L. Strong marine-derived nitrous acid (HONO) production observed in the coastal atmosphere of northern China. *Atmos. Environ.* **2021**, *244*, 117948.

(21) Cesari, D.; Amato, F.; Pandolfi, M.; Alastuey, A.; Querol, X.; Contini, D. An inter-comparison of $PM_{10}$ source apportionment using PCA and PMF receptor models in three European sites. *Environ. Sci. Pollut. Res.* **2016**, *23* (15), 15133−15148.

(22) Jolliffe, I. T. Principal Components in Regression Analysis. In *Principal component analysis*; Springer: New York, 2002; pp 167−195.

(23) Wilks, D. S. *Statistical methods in the atmospheric sciences*; Academic Press: New York, 2019.

(24) Langford, A. O.; Senff, C. J.; Banta, R. M.; Hardesty, R. M.; Alvarez, R. J.; Sandberg, S. P.; Darby, L. S. Regional and local background ozone in Houston during Texas Air Quality Study 2006. *J. Geophys. Res.: Atmos.* **2009**, *114* (D7), D00F12.

(25) Tokarek, T. W.; Odame-Ankrah, C. A.; Huo, J. A.; McLaren, R.; Lee, A. K. Y.; Adam, M. G.; Willis, M. D.; Abbatt, J. P. D.; Mihele, C.; Darlington, A.; Mittermeier, R. L.; Strawbridge, K.; Hayden, K. L.; Olfert, J. S.; Schnitzler, E. G.; Brownsey, D. K.; Assad, F. V.; Wentworth, G. R.; Tevlin, A. G.; Worthy, D. E. J.; Li, S. M.; Liggio, J.; Brook, J. R.; Osthoff, H. D. Principal component analysis of summertime ground site measurements in the Athabasca oil sands with a focus on analytically unresolved intermediate-volatility organic compounds. *Atmos. Chem. Phys.* **2018**, *18* (24), 17819−17841.

(26) Liu, Y. J.; Yang, Z.; Liu, Q. Y.; Qi, X. K.; Qu, J. M.; Zhang, S. M.; Wang, X. X.; Jia, K.; Zhu, M. H. Study on chemical components and sources of $PM_{2.5}$ during heavy air pollution periods at a suburban site in Beijing of China. *Atmos. Pollut. Res.* **2021**, *12* (4), 188−199.

(27) Acker, K.; Febo, A.; Trick, S.; Perrino, C.; Bruno, P.; Wiesen, P.; Möller, D.; Wieprecht, W.; Auel, R.; Giusto, M.; Geyer, A.; Platt, U.; Allegrini, I. Nitrous acid in the urban area of Rome. *Atmos. Environ.* **2006**, *40* (17), 3123−3133.

(28) Acker, K.; Möller, D.; Wieprecht, W.; Meixner, F. X.; Bohn, B.; Gilge, S.; Plass-Dülmer, C.; Berresheim, H. Strong daytime production of OH from $HNO_2$ at a rural mountain site. *Geophys. Res. Lett.* **2006**, *33* (2), 4.

(29) Acker, K.; Möller, D. Atmospheric variation of nitrous acid at different sites in Europe. *Environ. Chem.* **2007**, *4* (4), 242−255.

(30) Crilley, L. R.; Kramer, L. J.; Pope, F. D.; Reed, C.; Lee, J. D.; Carpenter, L. J.; Hollis, L. D. J.; Ball, S. M.; Bloss, W. J. Is the ocean surface a source of nitrous acid (HONO) in the marine boundary layer? *Atmos. Chem. Phys.* **2021**, *21* (24), 18213−18225.

(31) Cui, L. L.; Li, R.; Fu, H. B.; Li, Q.; Zhang, L. W.; George, C.; Chen, J. M. Formation features of nitrous acid in the offshore area of the East China Sea. *Sci. Total Environ.* **2019**, *682*, 138−150.

(32) Kerbrat, M.; Legrand, M.; Preunkert, S.; Gallée, H.; Kleffmann, J. Nitrous acid at Concordia (inland site) and Dumont d'Urville (coastal site), East Antarctica. *J. Geophys. Res.: Atmos.* **2012**, *117* (D8), n/a.

(33) Kleffmann, J.; Lorzer, J. C.; Wiesen, P.; Kern, C.; Trick, S.; Volkamer, R.; Rodenas, M.; Wirtz, K. Intercomparison of the DOAS and LOPAP techniques for the detection of nitrous acid (HONO). *Atmos. Environ.* **2006**, *40* (20), 3640−3652.

(34) Li, G.; Lei, W.; Zavala, M.; Volkamer, R.; Dusanter, S.; Stevens, P.; Molina, L. T. Impacts of HONO sources on the photochemistry in Mexico City during the MCMA-2006/MILAGO Campaign. *Atmos. Chem. Phys.* **2010**, *10* (14), 6551−6567.

(35) Li, X.; Brauers, T.; Haseler, R.; Bohn, B.; Fuchs, H.; Hofzumahaus, A.; Holland, F.; Lou, S.; Lu, K. D.; Rohrer, F.; Hu, M.; Zeng, L. M.; Zhang, Y. H.; Garland, R. M.; Su, H.; Nowak, A.; Wiedensohler, A.; Takegawa, N.; Shao, M.; Wahner, A. Exploring the atmospheric chemistry of nitrous acid (HONO) at a rural site in Southern China. *Atmos. Chem. Phys.* **2012**, *12* (3), 1497−1513.

(36) Liu, Y. L.; Nie, W.; Xu, Z.; Wang, T. Y.; Wang, R. X.; Li, Y. Y.; Wang, L.; Chi, X. G.; Ding, A. J. Semi-quantitative understanding of source contribution to nitrous acid (HONO) based on 1 year of continuous observation at the SORPES station in eastern China. *Atmos. Chem. Phys.* **2019**, *19* (20), 13289−13308.

(37) Meusel, H.; Kuhn, U.; Reiffs, A.; Mallik, C.; Harder, H.; Martinez, M.; Schuladen, J.; Bohn, B.; Parchatka, U.; Crowley, J. N.; Fischer, H.; Tomsche, L.; Novelli, A.; Hoffmann, T.; Janssen, R. H. H.; Hartogensis, O.; Pikridas, M.; Vrekoussis, M.; Bourtsoukidis, E.; Weber, B.; Lelieveld, J.; Williams, J.; Poschl, U.; Cheng, Y. F.; Su, H. Daytime formation of nitrous acid at a coastal remote site in Cyprus indicating a common ground source of atmospheric HONO and NO. *Atmos. Chem. Phys.* **2016**, *16* (22), 14475−14493.

(38) Nakashima, Y.; Sadanaga, Y.; Saito, S.; Hoshi, J.; Ueno, H. Contributions of vehicular emissions and secondary formation to nitrous acid concentrations in ambient urban air in Tokyo in the winter. *Sci. Total Environ.* **2017**, *592*, 178−186.

(39) Pusede, S. E.; VandenBoer, T. C.; Murphy, J. G.; Markovic, M. Z.; Young, C. J.; Veres, P. R.; Roberts, J. M.; Washenfelder, R. A.; Brown, S. S.; Ren, X. R.; Tsai, C.; Stutz, J.; Brune, W. H.; Browne, E. C.; Wooldridge, P. J.; Graham, A. R.; Weber, R.; Goldstein, A. H.; Dusanter, S.; Griffith, S. M.; Stevens, P. S.; Lefer, B. L.; Cohen, R. C. An Atmospheric Constraint on the NO₂ Dependence of Daytime Near-Surface Nitrous Acid (HONO). *Environ. Sci. Technol.* **2015**, *49* (21), 12774−12781.

(40) Reed, C.; Evans, M. J.; Crilley, L. R.; Bloss, W. J.; Sherwen, T.; Read, K. A.; Lee, J. D.; Carpenter, L. J. Evidence for renoxification in the tropical marine boundary layer. *Atmos. Chem. Phys.* **2017**, *17* (6), 4081−4092.

(41) Stutz, J.; Oh, H. J.; Whitlow, S. I.; Anderson, C.; Dibb, J. E.; Flynn, J. H.; Rappengluck, B.; Lefer, B. Simultaneous DOAS and mist-chamber IC measurements of HONO in Houston, TX. *Atmos. Environ.* **2010**, *44* (33), 4090−4098.

(42) VandenBoer, T. C.; Markovic, M. Z.; Sanders, J. E.; Ren, X.; Pusede, S. E.; Browne, E. C.; Cohen, R. C.; Zhang, L.; Thomas, J.; Brune, W. H.; Murphy, J. G. Evidence for a nitrous acid (HONO) reservoir at the ground surface in Bakersfield, CA, during CalNex 2010. *J. Geophys. Res.: Atmos.* **2014**, *119* (14), 9093−9106.

(43) Villena, G.; Wiesen, P.; Cantrell, C. A.; Flocke, F.; Fried, A.; Hall, S. R.; Hornbrook, R. S.; Knapp, D.; Kosciuch, E.; Mauldin, R. L.; McGrath, J. A.; Montzka, D.; Richter, D.; Ullmann, K.; Walega, J.; Weibring, P.; Weinheimer, A.; Staebler, R. M.; Liao, J.; Huey, L. G.; Kleffmann, J. Nitrous acid (HONO) during polar spring in Barrow, Alaska: A net source of OH radicals? *J. Geophys. Res.* **2011**, *116* (D14), D00R07.

(44) Wang, J.; Zhang, X.; Guo, J.; Wang, Z.; Zhang, M. Observation of nitrous acid (HONO) in Beijing, China: Seasonal variation, nocturnal formation and daytime budget. *Sci. Total Environ.* **2017**, *587−588*, 350−359.

(45) Wang, S. S.; Zhou, R.; Zhao, H.; Wang, Z. R.; Chen, L. M.; Zhou, B. Long-term observation of atmospheric nitrous acid (HONO) and its implication to local NO₂ levels in Shanghai, China. *Atmos. Environ.* **2013**, *77*, 718−724.

(46) Ye, C. X.; Heard, D. E.; Whalley, L. K. Evaluation of Novel Routes for NOₓ Formation in Remote Regions. *Environ. Sci. Technol.* **2017**, *51* (13), 7442−7449.

(47) Fu, X.; Wang, T.; Zhang, L.; Li, Q. Y.; Wang, Z.; Xia, M.; Yun, H.; Wang, W. H.; Yu, C.; Yue, D. L.; Zhou, Y.; Zheng, J. Y.; Han, R. The significant contribution of HONO to secondary pollutants during a severe winter pollution event in southern China. *Atmos. Chem. Phys.* **2019**, *19* (1), 1−14.

(48) Zhang, W. Q.; Tong, S. R.; Jia, C. H.; Wang, L. L.; Liu, B. X.; Tang, G. Q.; Ji, D. S.; Hu, B.; Liu, Z. R.; Li, W. R.; Wang, Z.; Liu, Y.; Wang, Y. S.; Ge, M. F. Different HONO Sources for Three Layers at the Urban Area of Beijing. *Environ. Sci. Technol.* **2020**, *54* (20), 12870−12880.

(49) Xue, C. Y.; Zhang, C. L.; Ye, C.; Liu, P. F.; Catoire, V.; Krysztofiak, G.; Chen, H.; Ren, Y. G.; Zhao, X. X.; Wang, J. H.; Zhang, F.; Zhang, C. X.; Zhang, J. W.; An, J. L.; Wang, T.; Chen, J.

(50) M.; Kleffmann, J.; Mellouki, A.; Mu, Y. J. HONO Budget and Its Role in Nitrate Formation in the Rural North China Plain. *Environ. Sci. Technol.* **2020**, *54* (18), 11048−11057.

(50) Huang, R. J.; Yang, L.; Cao, J. J.; Wang, Q. Y.; Tie, X. X.; Ho, K. F.; Shen, Z. X.; Zhang, R. J.; Li, G. H.; Zhu, C. S.; Zhang, N. N.; Dai, W. T.; Zhou, J. M.; Liu, S. X.; Chen, Y.; Chen, J.; O'Dowd, C. D. Concentration and sources of atmospheric nitrous acid (HONO) at an urban site in Western China. *Sci. Total Environ.* **2017**, *593*, 165−172.

(51) Zhang, W.; Tong, S.; Ge, M.; An, J.; Shi, Z.; Hou, S.; Xia, K.; Qu, Y.; Zhang, H.; Chu, B.; Sun, Y.; He, H. Variations and sources of nitrous acid (HONO) during a severe pollution episode in Beijing in winter 2016. *Sci. Total Environ.* **2019**, *648*, 253−262.
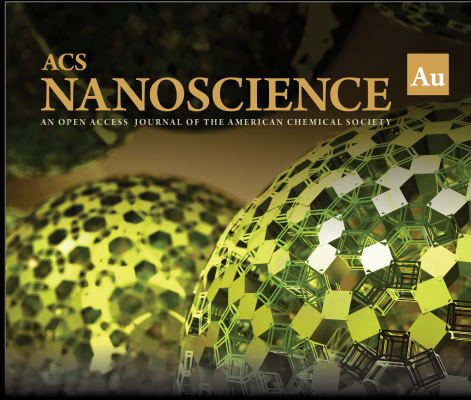
(52) Finlayson-Pitts, B. J.; Wingen, L. M.; Sumner, A. L.; Syomin, D.; Ramazan, K. A. The heterogeneous hydrolysis of NO₂ in laboratory systems and in outdoor and indoor atmospheres: An integrated mechanism. *Phys. Chem. Chem. Phys.* **2003**, *5* (2), 223−242.

(53) Zhou, X.; Huang, G.; Civerolo, K.; Roychowdhury, U.; Demerjian, K. L. Summertime observations of HONO, HCHO, and O₃ at the summit of Whiteface Mountain, New York. *J. Geophys. Res.: Atmos.* **2007**, *112* (D8), D08311.

(54) Cui, L. L.; Wang, S. X. Mapping the daily nitrous acid (HONO) concentrations across China during 2006−2017 through ensemble machine-learning algorithm. *Sci. Total Environ.* **2021**, *785*, 147325.

(55) Yang, W.; Yuan, H.; Han, C.; Yang, H.; Xue, X. Photochemical emissions of HONO, NO₂ and NO from the soil surface under simulated sunlight. *Atmos. Environ.* **2020**, *234*, 117596.

(56) Legrand, M.; Preunkert, S.; Frey, M.; Bartels-Rausch, T.; Kukui, A.; King, M. D.; Savarino, J.; Kerbrat, M.; Jourdain, B. Large mixing ratios of atmospheric nitrous acid (HONO) at Concordia (East Antarctic Plateau) in summer: a strong source from surface snow? *Atmos. Chem. Phys.* **2014**, *14* (18), 9963−9976.